ARTICLES

Connecting Structure to Infrared Spectra of Molecular and Autodissociated HCl−Water Aggregates†

Marco Masia,*,‡ Harald Forbert, and Dominik Marx

Lehrstuhl für Theoretische Chemie, Ruhr-Universität Bochum, D-44780 Bochum, Germany

Received: May 25, 2007; In Final Form: July 8, 2007

The properties of perdeuterated $HCl(H_2O)_n$ aggregates with $n = 1, 2, ..., 6$ water molecules are studied by means of ab initio molecular dynamics simulations. The specific focus is on the phenomenon of autodissociation of the acid HCl as a function of the microsolvation environment size. The calculations provide a basis for characterization in terms of autodissociation energetics as well as in terms of the impact of thermal fluctuations on structure including proton fluxionality and in terms of anharmonic infrared vibrational spectra. Structure stabilization is dominated by strong hydrogen bonds resulting in distinct topologies, which, in turn, heavily influence acid dissociation. The latter is favored for the first time when $n = 4$. In that case, three hydrogen bonds can be donated toward the chlorine while at the same time a hydronium core is perfectly solvated according to the eigencomplex motif. Hydrogen-bonding interactions between DCl and its solvating molecules affect the dynamical behavior of the D−Cl bond significantly. This can be seen by the onset of fluxionality and an emerging tendency toward proton transfer for the larger clusters. Connecting IR spectra to structural information is possible by exploiting the following observations. Zwitterionic species show characteristic differences in the hydronium region, whereas the D−Cl stretching regime is useful to distinguish neutral aggregates. Furthermore, in the case of fluxional protons large-amplitude motion leads to characteristic band shifts and significant band broadening effects.

I. Introduction

Understanding the ionization processes of acids in water aggregates, ranging from small to large sizes, has gained much interest recently due to its impact on atmospheric chemistry, given, for instance, its role in ozone depletion in the Antarctic. It has been demonstrated that the production of Cl_2 and HNO_3 (which will then react with ozone) in the stratosphere is due to the reaction of $ClONO_2$ with HCl and water and that this reaction is catalyzed on the surfaces of micrometer-sized ice particles found in polar stratospheric clouds.[1−4] In particular, because acid autodissociation followed by the formation of solvated ionic species can play an important role in the first steps of nucleation in atmospheric clusters, studies focus on determining the minimum number *n* of water molecules required for the onset of dissociation.[5]

Both experimental[3,5−8] and theoretical[9−23] studies on hydrated HX (X = F, Cl, Br, and I) clusters suggest that this number depends on the halide: For HI and HBr, three water molecules are sufficient for autodissociation, while in the cases of HCl and HF at least four water molecules are needed. At this value the dissociated zwitterionic structure $H^+(H_2O)_4Cl^-$ is more stable than the molecular one $HCl(H_2O)_4$; note that our nomenclature $H^+(H_2O)_nCl^-$ does not imply a particular solvation pattern of the detached proton. The other halide acids show the same trend; the only exception is HF because its undissociated form seems to be stable for $n < 11$.[23] Thermodynamically, in the case of HCl, higher temperatures stabilize the molecular structure for $n = 4$ due to fluctuations (entropy), and as a result, the autodissociation limit is shifted toward larger clusters.[9] However, for $n = 4$, CCSD(T) calculations[19] provide an autodissociation scenario that involves three intermediates and two rather high barriers (3.92 and 7.78 kcal mol^{-1}). Thus, autoionization of small neutral HCl/water aggregates may be kinetically hindered or even prevented at sufficiently low temperatures, for example, in ultracold superfluid helium nanodroplets.[24,25] For $n = 5$, however, acid dissociation should become a barrierless process. In fact, CCSD(T) calculations[19] showed that the isomerization process of $n = 5$ must overcome only two small activation barriers, the highest one being ∼0.7 kcal mol^{-1}. Note that later a different undissociated $n = 5$ cluster has been identified to be the most stable isomer,[21] which is the one considered in the present study. For $HBr(H_2O)_n$ clusters ($n = 4$ or 5), a similar behavior has been found using PBE/TZVP calculations;[22] this system shows even higher barriers than those found for HCl dissociation. Recently, much effort has been devoted to understanding the role of microsolvation on acid dissociation in water.[26−30] Apart from these interests, water−induced acid dissociation is at the heart of many proton-transfer processes[31] occurring in aqueous media. Even though aspects of such processes can be faithfully studied with static quantum chemical calculations, some features are most directly

† Part of the "Giacinto Scoles Festschrift".

* Author to whom correspondence should be addressed. E-mail: marco.masia@uniss.it.

‡ Present address: Dipartimento di Chimica, Università di Sassari, Via Vienna 2, I-07100 Sassari, Italy.

10.1021/jp0740494 CCC: $37.00
Published on Web 10/04/2007

revealed by ab initio molecular dynamics simulations because they enable one to relate most directly structural properties (e.g., solvation of the proton) to dynamical ones (e.g., IR spectra). Moreover, static calculations give information only on the equilibrium structure r_{eq} as defined by the minimum of the potential energy surface, which is not directly accessible in any experiment. However, the most probable structure r_P and the average structure $\langle r \rangle$ can be easily obtained from ab initio molecular dynamics trajectories by evaluating probability distribution functions. They are much more appropriate concepts to take into account vibrational effects on molecular structure,[32] which are intimately connected to band shifting and line shape broadening in IR spectra.

Experimentally, mainly IR and Raman vibrational spectroscopy are used as probes to understand the molecular details of the structure of acid-doped clusters, which are still poorly understood. Even more so, virtually nothing is known about the dissociation dynamics, pathways, and mechanisms that connect stable molecular and zwitterionic variants of such clusters for a given *n*. A prime difficulty of many experimental approaches is the clean interpretation of the spectra and the respective peak shifts. This is due to the presence of a distribution of cluster sizes *n* in the samples. Furthermore, experimental results can be affected by two additional phenomena: (i) Clusters are often obtained under nonequilibrium conditions, and kinetically favored (metastable) species can be formed in some cases, and (ii) a rigorous size assignment is more challenging for neutral hydrogen-bonded clusters rather than for ionic species.[6] So far, major efforts in understanding the spectra have allowed us to safely assign the bands of clusters with $n = 1$ and 2 water molecules, while for $n = 3$ and 4 only incomplete and speculative assignments are available.[5−8]

In the present contribution, we focus on the role of hydrogen bonds in the stabilization of neutral and zwitterionic aggregates of hydrogen chloride and water, $HCl(H_2O)_n$, in the size range from $n = 1$ to 6, extensively using ab initio molecular dynamics simulations of the perdeuterated species. The core of this investigation is the extent to which the particular hydrogen-bonding topology affects the vibrational spectra. Additionally, we provide tentative assignments for these spectra. The paper is organized as follows: Computational details and methods are explained in section II; the next section contains the results in three subsections concerning energetic properties, structural properties, and the analysis of infrared spectra. We will summarize the main results in the Conclusions and Outlook section.

II. Computational Details

A. Simulation Setup. Structure optimization, harmonic vibrational analysis (VA), Car−Parrinello (CP),[33] and Born−Oppenheimer (BO) ab initio molecular dynamics were performed using the CPMD package.[34,35] The BLYP functional[36,37] was chosen together with norm-conserving pseudopotentials[38] with a plane wave cutoff of 70 Ry. The supercell for all calculations was a cubic box of 20.0 Å in length, and cluster boundary conditions were applied[39] to properly treat these isolated systems. All dynamic simulations were performed in the canonical ensemble at 50 K. Nosé−Hoover chains (NHCs)[40] were applied to keep the kinetic energy of the nuclei (as well as the fictitious kinetic energy of the orbitals in the case of CP propagation) constant. Note that NHC dynamics can be used to generate dynamical information if appropriate care is taken.[41] The isotope masses of Cl, O, and D were set respectively to 34.9688, 15.9994, and 2.0141 amu, while the fictitious mass parameter for the orbitals, μ, was set to 760 a.u.; note that for simplicity the notation "proton'' and the notation "H'' are occasionally used when referring to our simulation results obtained with perdeuterated systems. As is well-understood, using a finite μ will red-shift vibrational frequencies by increasing the effective mass of the moving atoms.[35,42] This shift can be either corrected approximately[42−44] or quantified by directly comparing CP to BO spectra as done here.

Starting from the optimized structures, the systems were equilibrated by thermostating each degree of freedom with a separate NHC for ∼1.5 ps to enforce energy equipartitioning of even stiff intramolecular modes[45] followed by further equilibration for ∼0.7 ps using one NHC. This equilibration was followed by production runs of 15 ps from which all reported quantities were obtained; in the case of BO the total simulated time was 10 ps. During all simulations the total linear and angular momenta were corrected to zero as described in subsection 2.2 of ref 46.

For a deeper electronic structure analysis, maximally localized Wannier orbitals[47−49] were computed every 30 a.u. along the trajectory. Their (charge) centers provide some kind of measure of the location of an electron in space that allows us to define (effective local) dipole moments of molecular fragments of an aggregate, μ_I, that add up to the total dipole moment, $M(t) = \sum_I^{N^{mol}} \mu_I(t)$. Within this approach, the dipole moment of a molecule *I* is given by

$$\mu_I = \sum_{j=1}^{N_I^{ion}} q_j^{ion}\, \mathbf{r}_j^{ion} + \sum_{k=1}^{N_I^{el}} q_k^{el}\, \mathbf{r}_k^{el} = \mu_I^{ion} + \mu_I^{el} \qquad (1)$$

where q_j^{ion} is the core charge of the *j*th nucleus at position $\mathbf{r}_j^{ion}(t)$, $q_k^{el} = -2e$ is the charge of closed-shell Wannier orbitals holding two electrons with centers at $\mathbf{r}_k^{el}(t)$, and N_I^{ion} and N_I^{el} are the number of ions and Wannier centers that are assigned to the *I*th molecule.

B. Infrared Spectra and Frequency Assignment. Infrared spectra were obtained straightforwardly as the fast Fourier transform (FFT) of the classical autocorrelation function $C_{cl}(t)$ of the total dipole moment *M* (including both nuclear and electronic contributions)

$$S_{cl}(\omega) = \mathrm{FFT}[C_{cl}(t)] = \frac{1}{2\pi}\int_{-\infty}^{\infty} \mathrm{d}t\, \exp(-i\omega t)\langle M(0)M(t)\rangle_{cl} \qquad (2)$$

where $S_{cl}(\omega)$ is the classical line shape function.[50−52] The absorption cross-section $I(\omega)$ as measured in experiments is given by

$$I(\omega) = \frac{4\pi^2\omega}{\hbar c n(\omega)}(1 - \exp[-\beta\hbar\omega])S(\omega) \qquad (3)$$

where $S(\omega)$ is the quantum line shape function (*c* is the speed of light and $n(\omega)$ is the frequency-dependent refractive index assumed to be unity). Quantum correction factors (QCFs) to the classical line shape functions are needed to approximate the true quantum line shape function and thus IR spectra.[53] In particular, the so-called high-temperature (or harmonic) QCF

$$I_{qc}(\omega) = \frac{4\pi^2\beta\omega^2}{c} S_{cl}(\omega) \qquad (4)$$

is found to work well for anharmonic vibrational spectra and hydrogen-bonded systems.[46,53−56]

Assignment of the most prominent IR peaks was achieved using four different approaches:

1. Standard normal modes. Harmonic VA[57] was used to calculate the harmonic frequencies. Once translations and rotations are subtracted, a set of $(3N - 6)$ $3N$-dimensional orthonormal eigenvectors e_i (N = number of atoms) are obtained that describe the motion of the independent vibrational modes.

2. Projected normal modes. During the dynamical evolution of the system, we calculated the mass-weighted displacement, $ds(t) = \mathcal{M}(x(t) - x_{eq})$ of the trajectory with respect to the equilibrium structure. Here $x(t)$ is the configuration at time t, x_{eq} is the equilibrium structure, and $\mathcal{M}$ is the diagonal $3N \times 3N$ matrix of the square root of the nuclear masses. The projection $P_i(t) = ds(t)\, e_i$ can be considered as the time evolution of the ith normal mode.

3. Effective modes. A sophisticated general method was recently developed[58] for obtaining effective normal modes at finite temperatures that is based on a localization criterion for the transformed velocity autocorrelation functions of the effective modes.

4. Molecular dipole moments. Local molecular dipole moments $\mu_I(t)$ in the aggregates were obtained as a sum of contributions from both ions and electrons (see subsection IIA, eq 1). Fourier transformation of the auto- and cross-correlation functions of these approximate molecular dipole moments is useful for decomposing and thus assigning the total spectra. However, it must be remembered that the total spectrum is not just the sum of such (effective) single-molecule contributions. In particular, the autocorrelation function of the decomposed total dipole moment, i.e., $M(t) = \sum_I^{N^{mol}} \mu_I(t)$ where N^{mol} is the number of molecular fragments into which the aggregate has been decomposed, as needed in eq 2 reads

$$\langle M(0)M(t)\rangle_{cl} = \sum_I \langle \mu_I(0)\mu_I(t)\rangle_{cl} + \sum_{I,J\neq I} \langle \mu_I(0)\mu_J(t)\rangle_{cl} = \sum_I C_{II}(t) + \sum_{I,J\neq I} C_{IJ}(t) \quad (5)$$

where the diagonal and off-diagonal terms represent auto- and cross-correlations, respectively. In the total spectrum the cross-correlation is only important for neighboring molecules I and J because it tends to vanish as their intermolecular distance increases. Thus, such analysis allows one to understand clearly which vibrations are independent and which are coupled.

Finally, we stress that all of these methods are limited by some kind of approximation, but when used together they are capable of yielding complementary information that allows a safe assignment of even complex vibrational spectra.

III. Results

A. Energetic Properties: Formation Energies and Autodissociation Energies. An overview of the optimized structures corresponding to all clusters is provided by Figure 1, including the molecular and dissociated species. Previous studies[18−21] have shown that the number of metastable isomers increases strongly with n as expected. Here we have restricted our focus to the lowest−energy neutral and zwitterionic cluster for each size n.

In general, hydrogen bonds (in particular their topological arrangement) are vital for stabilizing these cluster structures as a function of size, as we will discuss below. For the specific cases studied here, cluster stabilization due to hydrogen bonds can be assessed from Table 1, where we report both the formation energy for each cluster and the energy difference between dissociated and undissociated isomers of the same cluster size as computed from the respective optimized structures. In particular, when a water molecule is added to a cluster, the energy gain is not constant along the series. A comparison of the present results with previous ab initio calculations[18−21] is also shown.

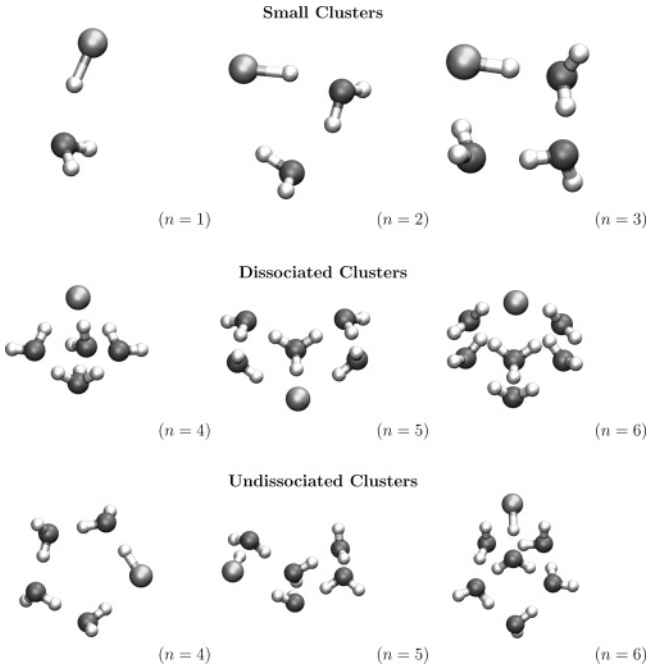

Figure 1. Structures of the studied clusters.

If we first focus our attention on previous studies, then we find that, depending on the electronic structure approach used, the values of all cluster formation energies show discrepancies. The largest difference among the methods is as large as ∼5 kcal mol^{-1}, which is well within the range of the energetic contribution of a single hydrogen bond. If we consider our density functional values, then we find that the difference in energy with published results grows linearly with cluster size. These discrepancies might be due to the basis set superposition error (BSSE) occurring when using localized basis sets, which gives a spurious contribution to the hydrogen-bonded interaction energies,[59] whereas our plane wave basis is free of BSSE.[35] As far as we know, none of the reference data[18−21] reported in Table 1 is corrected for BSSE by using, for example, the counterpoise correction scheme. Our quantum chemical calculations on the $n = 1$ cluster show that the BSSE is 0.91 kcal mol^{-1} when a MP2/aug-cc-pVDZ model is used. Moreover, after having optimized the structure with the counterpoise correction, the formation energy is much closer to our plane wave result. The BSSE does not affect isomerization energies as much, because the structures to be compared are rather similar. This is in accord with the agreement between quantum chemical calculations using Gaussian basis sets and our plane wave calculations, when we consider the energy difference between two isomers of a given cluster size.

We note in passing that care must be taken when comparing numbers from different publications that rely on standard basis set sizes and correlation treatments when dealing with systems subject to strong nonbonded interactions such as the aggregates considered here. This can be demonstrated easily by performing standard[60] single-point total energy calculations on given structures for the two (undissociated and the dissociated) $n = 4$ isomers to obtain a feeling for the dependence of the energy difference both on the correlation treatment and on the basis set (Table 2). We see that while the BLYP and B3LYP

TABLE 1: Formation Energies (Not Corrected for BSSE) for Each Cluster and Energy Differences between Undissociated (U) and Dissociated (D) Clusters (i.e., Isomerization Energies) as Obtained in This and Previous Works[a]

	this work	ref 21		ref 20		ref 19	ref 18	
n	(a)	(b)	(c)	(d)	(e)	(g)	(h)	(i)
1	−4.68	−6.21	−6.50	−6.02	−6.66			
2	−12.76	−15.21	−15.13	−14.96	−16.16			
3	−23.57	−26.47	−27.08	−26.82	−28.84			
4U	−32.18	−35.72	−37.37	−37.13	−39.69			
4D	−34.87	−38.45	−38.27	−37.16	−42.35			
5U	−39.16	−46.21	−47.22					
5D	−46.66	−51.34	−52.17	−50.68				
6U	−49.18	−59.68	−59.06					
6D	−55.63	−66.44	−63.67					
4D − 4U	−2.69	−2.73	−0.90	−0.03	−2.66	−2.43	−0.7	−3.2
5D − 5U	−7.50	−5.13	−6.89					
6D − 6U	−6.45	−6.76	−4.61					

[a] All values are given in kcal mol^{-1}. Electronic structure methods used: (a) BLYP/plane waves (see section II for details); (b) MP2/aug-cc-pVDZ; (c) B3LYP/6-311++G**[sp]; (d) MP2/TVZP; (e) B3LYP/TVZP; (g) CCSD(T)/aug-cc-pVDZ; (h) B3LYP/D95++(p,d); (i) B3LYP/D95(p,d).

TABLE 2: Dependence of the 4D − 4U Energy Difference on the Electronic Structure Method and Basis Set Used[a]

basis set	BLYP	B3LYP	MP2
cc-pVDZ	−8.72	−8.18	−5.33
cc-pVTZ	−3.01	−3.41	−4.36
cc-pVQZ	−1.40	−2.01	−3.73
aug-cc-pVDZ	−1.60	−2.31	−2.70
aug-cc-pVTZ	−0.53	−1.47	−3.43
aug-cc-pVQZ	−0.39	−1.24	−3.54

[a] No correction was applied for the BSSE. All values are in kcal mol^{-1}.

functionals display the same trend, i.e., the energy difference decreases as the basis set increases, the MP2 calculations show exactly the opposite behavior. For the sake of comparison, we also investigated the dependence of this isomerization energy on the basis set size for our plane waves by changing the plane wave cutoff value. In this case we used BLYP with pseudopotentials. Upon increasing the plane wave kinetic energy cutoff from 70 to 200 Ry, we found that the energy difference again decreases from −2.7 to the plateau value of −1.6 kcal mol^{-1}, which is well within the typical range of standard ab initio calculations for this quantity.

In conclusion, with respect to the electronic structure method, we note that the present generalized gradient approximation density functional pseudopotential/plane wave results are of a quality that is similar to that obtained in other state-of-the-art studies of aggregates in this size range. This gives us confidence to use the identical electronic structure method as employed for this static treatment in the framework of dynamical ab initio simulations to probe the effect of fluctuations as well as to compute and to assign anharmonically coupled IR spectra of both neutral (undissociated) and zwitterionic (dissociated) aggregates.

B. Structural Properties: Static Structures and Thermal Fluctuation Effects. From Figure 1, it can be seen that for $2 \leq n \leq 4$ the undissociated isomers feature an almost planar ring structure. In these cases each water molecule acts at the same time as a donor and an acceptor of one hydrogen bond. For $n = 5$ and 6 the complexity clearly increases: The planarity of the structure is lost, and some water molecules donate or accept more than one hydrogen bond. Dissociated clusters exhibit quite symmetrical structures around the hydronium ion. All of them have a three-dimensional topology, which makes a higher number of hydrogen bonds possible to stabilize the zwitterionic form. Three is the minimum number of water molecules that can stabilize a dissociated HCl molecule; however only when $n \geq 4$ does this zwitterionic isomer become favored energetically.[18−21]

For $n = 4$ the zwitterionic form has the shape of a trigonal bipyramid where Cl^- and H_3O^+ form the vertices and three water molecules form bridges between the two charged species. This topology can be understood as an eigencation $H_3O^+(H_2O)_3$ (see, for example, ref 31) with a hydronium core donating three hydrogen bonds, which simultaneously assures proper anionic solvation of the Cl^- counterion. In stark contrast, for $n = 5$, there is no such bridge between the chloride and the hydronium, which is now hydrogen-bonded directly to the anion itself and to two water molecules. In the dissociated structure of the $n = 6$ aggregate, the hydronium is again far away from the chloride, and it "shares'' one hydrogen with another water, thus approaching somewhat the bonding motif of a Zundel cation $[H_2O\cdots H\cdots OH_2]^+$ (see, for example, ref 31).

Besides the energetic parameters reported in Table 1 and discussed in the previous subsection, other criteria should be chosen to study the progression of hydrogen bonding. As commonly done, we use the distance D between the donor and the acceptor heavy atoms, the distance d between the hydrogen (i.e., deuterium) and the acceptor, and the angle ϕ between the two vectors joining the donor heavy atom to the hydrogen and to the acceptor, respectively. A structure is considered as hydrogen-bonded if and only if all three parameters are below a certain threshold value; in the case of water−water it is accepted to use $D < 3.6$ Å, $d < 2.4$ Å, and $\phi < 30°$ according to refs 61 and 62. There is also a general connection between directionality and strength of hydrogen bonds: the bridging hydrogen will tend toward the line connecting the heavy atoms. As a rule of thumb, the closer to linearity the hydrogen bond is, i.e., when $\phi \approx 0°$, the stronger it is, because this arrangement optimizes the electrostatic interaction.[63,64] Moreover, at a given value of the angle, the hydrogen bond is considered stronger if D and/or d are smaller.[63] For the clusters studied, we found that all of the above conditions are satisfied, the largest values for D and ϕ being 3.2 Å and 19°, respectively, which is much lower than required. Considering that most of the hydrogen bonds found are almost linear, the short distances between the heavy atoms suggest that the hydrogen bonds are quite strong.

Understanding the main structural properties of the clusters will be useful to help explain the microsolvation pattern of DCl or Cl^- as well as dynamical properties of the clusters such as isomerization pathways and mechanisms. To achieve this, besides the strength of hydrogen bonds, the coordination of chlorine when DCl is either dissociated or undissociated and the coordination of the excess proton in dissociated clusters

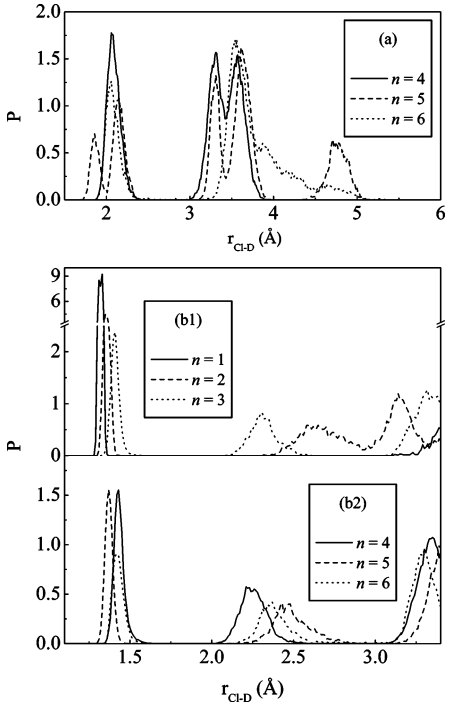

Figure 2. Probability distribution functions of the Cl−D distance for the (a) dissociated and (b1 and b2) undissociated clusters.

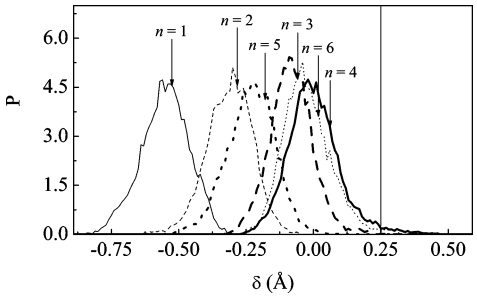

Figure 3. Probability distribution function of the asymmetric stretch coordinate δ for all undissociated clusters. Distinct line types are used to easily differentiate the data for different cluster sizes. Arrows indicate the value of the coordinate δ_{eq} at the static equilibrium structure for each cluster size (see also Table 3). As discussed in the text, the vertical solid line at $\delta_{sep} = 0.25$ Å represents the separatrix between the neutral and the zwitterionic species.

constitute two key points for the assignment of vibrational spectra. In Figure 2, we show the probability distribution function for the Cl−D distances in dissociated clusters in panel a and compare them to undissociated clusters in panels b1 and b2. For dissociated clusters, we observe only a few peaks due to the high symmetry of the structures. For $n = 4$, there are three different classes of deuterium atoms: (1) the three coordinating the anion with an average distance of ∼2.1 Å (first peak), (2) the three belonging to the hydronium, which are hydrogen-bonded to the bridging waters in terms of an eigen-solvation pattern (second peak, average distance ≈ 3.3 Å), and (3) three free deuteriums belonging to the bridging water molecules (third peak, average distance ≈ 3.6 Å). In this case, all three bridging waters are simultaneously donor and acceptor sites for hydrogen bonds.

For the larger $n = 5$ aggregate, we find two more types of deuterium atoms. The first two peaks correspond to three deuterium atoms coordinating the anion; two of them belong to the two hydrogen-bonded donating waters (average distance ≈ 2.16 Å), and one stems from the hydronium (average distance ≈ 1.88 Å). The third peak (average distance ≈ 3.3 Å) represents

TABLE 3: Average Values of the Hydrogen-Bond Parameters *D*, *d*, and ϕ as Well as δ for the Cl−D···O Interaction in Undissociated Clusters Obtained from Our Ab Initio Simulations[a]

n	*D* (Å)	*d* (Å)	ϕ (deg)	δ (Å)	δ_{eq} (Å)	$\delta^{\dagger}$ (Å)
1	3.20 (1.79)	1.88 (1.37)	5.1 (2.3)	−0.550 (0.089)	−0.524	−0.544
2	3.02 (1.74)	1.68 (1.30)	7.9 (2.8)	−0.311 (0.085)	−0.282	−0.387
3	2.92 (1.71)	1.50 (1.22)	3.3 (1.8)	−0.082 (0.080)	−0.057	−0.234
4	2.88 (1.70)	1.44 (1.20)	2.3 (1.5)	0.002 (0.098)	0.060	−0.183
5	2.99 (1.73)	1.61 (1.27)	3.3 (1.8)	−0.232 (0.089)	−0.179	−0.333
6	2.90 (1.70)	1.46 (1.21)	2.9 (1.7)	−0.023 (0.090)	0.017	−0.131

[a] The respective root-mean-square deviations are reported in parentheses. $\delta^{\dagger}$ is the value obtained in ab initio calculations at the MP2/aug-cc-pVDZ level.[21]

the other two deuteriums of the hydronium. Contrary to what happens with the $n = 4$ cluster, in this case the hydronium has two different kinds of deuterium atoms: one is hydrogen-bonded to the chloride, from which the mean distance is ∼1.9 Å, whereas the other two are involved in hydrogen bonds with water molecules and are much closer to the accepting oxygen (average distance ≈ 1.5 Å). The last two peaks in the probability distribution function come from other deuterium atoms that are involved in hydrogen bonds with either other water molecules or those that are free.

Passing to the $n = 6$ cluster we lose the high symmetry of the previous species. In this case, again, both the chloride and the hydronium are coordinated by three water molecules. The average D−Cl distance for the coordinating deuterium atoms (first peak) is ∼2.1 Å. Even if it is not appreciable in the probability distribution function, one deuterium stays, on average, further than the other two by ∼0.05 Å, and the O−D−Cl angle is ∼4° larger, suggesting that this hydrogen bond is not as strong as the other two. The charge defect resides on a water molecule where one deuterium stays at a very short distance from another water oxygen (∼1.48 Å); in spite of this no real proton-transfer event to the water has been recorded along the dynamical ab initio trajectory that underlies these probability distribution functions.

In the case of the undissociated clusters, we can devise three different regions according to panels b1 and b2 of Figure 2. The first represents the probability distribution function of the deuterium bonded to the chloride, the second represents all deuteriums that are in the first coordination shell of the chloride, and the third one is not important for the current analysis. In the first region we notice that the most probable distance of the nearest deuterium does not follow a monotonous trend as the size *n* increases. As a matter of fact, for $n = 1$ we have the shortest distance (∼1.33 Å) followed by $n = 2$, $n = 5$, $n = 3$, $n = 6$, and $n = 4$ (the most probable distances being ∼1.35, ∼1.37, ∼1.41, ∼1.42, and ∼1.43 Å, respectively). For easy reference the average values of the three parameters describing this particular hydrogen bond are compiled in Table 3 for each cluster. We see that this irregular trend concerning the size evolution of the covalent distance D−Cl is mirrored by the hydrogen-bond parameters as well. Moreover, because the hydrogen bond tends to linearity for $n = 4$ and $n = 6$ clusters and because both *d* and *D* show significant fluctuations, the joint probability distribution function of these three parameters can convey additional information about a possible fluxional behavior of the positive charge defect. As is customarily done, we use the asymmetric stretch coordinate $\delta = R_{Cl-D} - R_{D-O}$ as an order parameter to monitor deuterium movement and eventually proton transfer (see Figure 3 for the corresponding $P(\delta)$ distribution functions; the arrows indicate the values δ_{eq} at the corresponding equilibrium structures). Note that, because

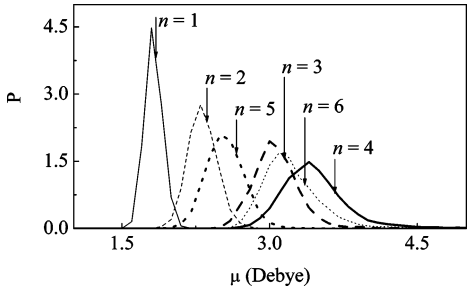

Figure 4. Probability distribution function of the local molecular dipole moment of the HCl fragment for all undissociated clusters. The line types are the same as in Figure 3. Arrows indicate the value of this dipole moment μ_{eq} at the static equilibrium structure for each cluster size.

the two heavy atoms have different van der Waals radii,[65] the value of the asymmetric stretch coordinate δ_{sep} that separates the state with dissociated HCl from the undissociated case is not centered around zero, but it is shifted toward positive values; also note that $\delta < \delta_{sep} = 0.25$ Å implies that the deuterium is closer to the chloride rather than to the oxygen and vice versa. It can be seen that for $n = 4$, $n = 6$, and also $n = 3$ there is a finite (albeit small) probability to cross this separating value δ_{sep}, marked by the vertical solid line, thus indicating that there are fluctuations present that "center'' this hydrogen bond. The trend found for the clusters with $n = 1$, 2, and 5 agrees with the behavior described above for the Cl−D···O hydrogen bond. In Table 3, we compile the average values and the root-mean-square deviation of δ as obtained from dynamical simulations to compare them to the equilibrium values calculated from the optimized static structures. In the last column, the equilibrium value found with high-level ab initio calculations is also reported; it can be seen that the trend is the same as that for our plane wave calculations. Note that in all cases thermal fluctuations shift this value toward smaller values with respect to the corresponding equilibrium values, i.e., closer to the chloride.

Coming back to the inspection of panels b1 and b2 of Figure 2, we notice that the second region of the Cl−D probability distribution function shows a completely different trend compared to the first region. In this case, for $n = 4$ the deuterium is located closer to the chloride (∼2.27 Å), and then we find $n = 3$, $n = 6$, $n = 5$, and $n = 2$ in succession (with ∼2.33, ∼2.39, ∼2.50, and ∼2.71 Å, respectively); it should be noted that the distribution functions of this first shell are very broad and thus feature large root-mean-square deviations (of 1.51, 1.52, 1.55, 1.58, and 1.64 Å following the order in the above sequence).

The influence of the environment around each molecule in the aggregate can be easily quantified by the change of its local dipole moment as obtained from Wannier decomposition of the electronic structure. The probability distribution function of the DCl molecular dipole moment for every undissociated cluster, μ_{DCl}, is shown in Figure 4; arrows mark these dipoles from static equilibrium structures. The trend is clearly the same as that found for $P(\delta)$; namely, the average dipole moment increases as the D−Cl bond becomes weaker. Furthermore, the distribution functions become broader as a consequence of fluctuations, which also shifts the most probable dipole moments (i.e., the maxima of the distributions) to smaller values compared to the respective equilibrium structures. The very same conclusion can be drawn when the water molecules that accept the DCl deuterium are considered.

C. Infrared Spectra. Infrared spectroscopy is commonly used as an experimental probe to investigate inter- and intramolecular interactions. However, the assignment of frequencies in floppy systems such as molecular clusters and aggregates is not always straightforward. Thus, deeper insights into structural and dynamical features obtained from simulations might be helpful after having connected directly theoretical to experimental IR spectra; note that most of the spectra are reported for the perdeuterated species.

TABLE 4: Effect of Isotopic Substitution in Experiment, Harmonic Vibrational Analysis (VA), Born−Oppenheimer (BO), and Car−Parrinello (CP) Molecular Dynamics Calculations for Hydrogen Chloride and Water[a]

			H_2O			D_2O		
	HCl	DCl	ν_1	ν_2	ν_3	ν_1	ν_2	ν_3
expt.	2886	2091	1595	3657	3756	1178	2671	2788
VA	2808	2014	1624	3519	3620	1189	2536	2651
BO	2780	1986	1578	3496	3597	1175	2518	2630
CP	2693	1929	1560	3366	3462	1142	2415	2519

[a] All values are given in cm^{-1}.

TABLE 5: Effect of Isotopic Substitution in Experiment, Harmonic Vibrational Analysis (VA), Born−Oppenheimer (BO), and Car−Parrinello (CP) Molecular Dynamics Calculations for the $n = 1$ Cluster[a]

	$HCl(H_2O)$				$DCl(D_2O)$			
	ν_6	ν_7	ν_8	ν_9	ν_6	ν_7	ν_8	ν_9
expt.		2723				1976		
VA	1619	2475	3503	3601	1185	1777	2524	2638
BO	1586	2467	3487	3585	1159	1776	2516	2624
CP	1551	2401	3364	3459	1138	1730	2417	2517

[a] All values are given in cm^{-1}.

1. Water Monomer, DCl Molecule, and n = 1 Dimer Cluster: Gauging the Calculations. These three systems constitute benchmarks for comparing numerical results with experiment. Hydrogen chloride has a single vibrational mode, i.e., the D−Cl stretch. Water has three normal modes (i.e., H−O−H bending (ν_1) and O−H symmetric (ν_2) and asymmetric (ν_3) stretching) whereas the (undissociated) $n = 1$ cluster, DCl-(D_2O), has nine such modes (i.e., H−O−H bending (ν_6), H−Cl stretching (ν_7), O−H symmetric (ν_8), and asymmetric (ν_9) stretching). In Tables 4 and 5, we compare the frequencies obtained for these three systems in experiments (see refs 7, 8, and 66 and references cited therein) to those obtained theoretically using the harmonic analysis and with both CP and BO ab initio molecular dynamics not only for the perdeuterated but also for the light species. The most trivial characteristic is that all frequencies, after isotopic substitution, are shifted to lower wavenumbers by a factor of ∼0.72. An estimate of the "exact'' factor for each normal mode is given by the ratio $R_i = \nu_i^H/\nu_i^D$, where ν_i^H and ν_i^D are the frequencies obtained by vibrational analysis of the ith normal mode for the hydrogenated and deuterated complexes, respectively. If we multiply the relative results obtained for deuterium with CP and BO by R, then we obtain a fairly good approximation of the results with hydrogen atoms (the largest deviation being only ∼0.3 %). In the tables containing the vibrational assignments of the simulated spectra of the larger clusters, we use the same method to estimate the values of fully hydrogenated systems. A further red shift is also evident in the CP calculations when compared to the corresponding BO simulations; this is a well-known inertia effect,[35,42] due to the introduction of a finite fictitious mass for the orbital degrees of freedom, which can be corrected.[42−44] Here, we quantify this shift most directly by comparison to BO spectra, which are not affected by this phenomenon.

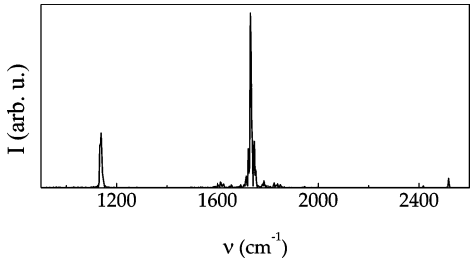

Figure 5. Vibrational spectrum for the $n = 1$ cluster (see subsection IIIC1 and Table 5 for the mode assignment).

A one-to-one comparison of each frequency of the harmonic vibrational analysis and of the BO simulations clearly shows that the difference is on the order of only a few wavenumbers. Comparison with experiment also shows that our computational methods tend to overestimate the shifts in frequencies between the heterodimer cluster and the two gas-phase monomers. The DCl stretching vibration, for example, is red-shifted by −199 cm^{-1} in the CP simulations, −210 cm^{-1} in BO, and −237 cm^{-1} in the harmonic vibrational analysis, whereas the experimental shift is only −115 cm^{-1}-.[6−8] This discrepancy appears to be substantial, but it is of the same order of magnitude as that obtained in previous calculations.[6,8,21] In particular, a study on small HCl− and HBr−solvent complexes[8] found that the calculated microsolvation shift depends both on the correlation treatment used and on the size of the basis set; the best estimate was obtained with −136 cm^{-1}, whereby B3LYP and MP2 with aug-cc-pV*x*Z (x = D, T, Q) basis sets lead to values ranging from −226 to −181 cm^{-1} in full accord with our findings. Thus, an important point that we would like to make is that as long as the D−Cl covalent bond is weakened by coordination of one water molecule, a significant red shift of the D−Cl stretching band is found in both experiment and theory. Moreover, the band is slightly broadened according to Figure 5 (cf. subsection IIIB in which we concluded that the deuterium is more labile and can show fluxional behavior for larger n values).

2. Clusters with n = 2 and 3: Band Assignments. These two clusters differ from the previous one because of their cyclic hydrogen-bonding structure that stabilizes the ring topology. The main signature of the hydrogen bonding is the shift of the O−D stretch to a lower frequency with respect to the non-hydrogen-bonded moieties (which are termed "free deuterium'' as is often the convention). In Table 6, we show the assignment of the most prominent peaks (see also Figure 6). It can be seen that the free hydrogen stretch frequencies are red-shifted by −50 to −100 cm^{-1}, while the shift of those hydrogen atoms involved in a hydrogen bond can even be more than 100 cm^{-1} larger. The first water molecule (i.e., the one involved in the strong interaction with DCl as a hydrogen-bond acceptor) experiences the most pronounced shifts for all stretch vibrations: 2269 and 2078 cm^{-1} for the hydrogen-bonded O−D stretch (for $n = 2$ and $n = 3$, respectively) and 2478 and 2473 cm^{-1} for the free hydrogen. This is due to the strong interaction with the deuterium of DCl, thereby weakening the O−D bond strength. Even if the perturbation is not that large in the other hydrogen-bonded water molecules, we notice that the red shifts are larger as the cluster size increases; this is another clue that points toward the cooperative effect of hydrogen bonding in these particular aggregates.

When we look at the D−Cl stretching frequency, both clusters show huge shifts relative to the isolated DCl monomer (−528 and −859 cm^{-1}, respectively, for $n = 2$ and $n = 3$). Previous B3LYP studies[7] on hydrogenated clusters are in agreement with our results (the reported values are −694 and −1199 cm^{-1}, which, after rescaling for perdeuterated clusters, become approximately −492 and −848 cm^{-1}, respectively). Despite this good agreement with previous quantum chemical results, these shifts are much more pronounced than those found in experiment,[7] in which the band origin is shifted only by −334 cm^{-1} for $n = 2$. Interestingly, experimental groups proposed different assignments of the $n = 3$ D−Cl stretch. While ref 5 found that the band for deuterated clusters is red-shifted by only 233 cm^{-1}, ref 8 speculates that this should be shifted by ∼500 wavenumbers. We have already noted in subsection IIIB that the D−Cl bond is more labile, leading to fluxional behavior as the size increases from $n = 2$ to 4. In accordance with this feature, we observe an increased red shift of the D−Cl stretch with respect to the $n = 2$ cluster. For this reason, we believe that our results support the interpretation proposed in ref 8, although it has been clearly stated therein that this assignment is only a tentative one. Thus, our data strongly suggest that the assignment of this particular band should be looked at again.

TABLE 6: Vibrational Assignment for the $n = 2$ and 3 Clusters' Spectra Calculated from the Equilibrium Structure (VA) and from the Dynamical Simulation at 50 K (CP, See Eq 2)[a]

NM	VA	assignment	CP
		$DCl(D_2O)_2$	
ν_{18}	1184 (1618)	D−O−D bend	1131 (1546)
ν_{19}	1191 (1633)	D−O−D bend	1135 (1557)
ν_{20}	1469 (2041)	D−Cl stretch	1448 (2012)
ν_{21}	2321 (3198)	Hb O−D stretch	2269 (3126)
ν_{22}	2474 (3422)	Hb O−D stretch	2386 (3300)
ν_{23}	2593 (3558)	free O−D stretch	2478 (3400)
ν_{24}	2613 (3576)	free O−D stretch	2498 (3418)
		$DCl(D_2O)_3$	
ν_{24}	1068 (1469)	D−Cl stretch	1117 (1536)
ν_{25}	1184 (1615)	D−O−D bend	1139 (1556)
ν_{26}	1191 (1632)	D−O−D bend	1142 (1566)
ν_{27}	1210 (1671)	D−O−D bend	1174 (1618)
ν_{28}	2050 (2817)	Hb O−D stretch	2078 (2853)
ν_{29}	2216 (3048)	Hb O−D stretch	2204 (3031)
ν_{30}	2374 (3274)	Hb O−D stretch	2312 (3188)
ν_{31}	2588 (3555)	free O−D stretch	2473 (3398)
ν_{32}	2602 (3570)	free O−D stretch	2486 (3411)
ν_{33}	2603 (3574)	free O−D stretch	2490 (3419)

[a] "Hb'' stands for hydrogen-bonded deuterium, in contrast to "free'' deuterium. The numbers in brackets in the VA column are the values obtained for the fully hydrogenated system. In the CP column, brackets are used for the estimated values of the same normal modes for the fully hydrogenated species (see subsection IIIC1 for details).

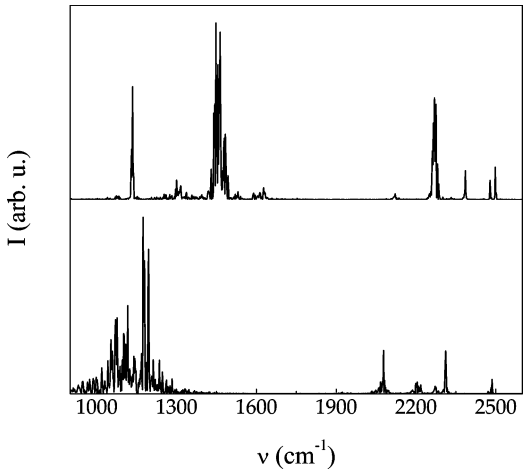

Figure 6. Vibrational spectra for $n = 2$ (upper graph) and $n = 3$ (lower graph) clusters (see Table 6 for the mode assignment).

TABLE 7: Vibrational Assignment for the Two Types of $n = 4$ Cluster[a]

	$[D(D_2O)_4]^+Cl^-$			$[DCl(D_2O)_4]$		
NM	VA	assignment	CP	VA	assignment	CP
ν_{29}	1163 (1594)	D−O−D bend	1121 (1536)	874 (1196)	D−Cl stretch	1027 (1405)
ν_{30}	1169 (1603)	D−O−D bend	1123 (1540)	887 (1236)	D_2O twisting	818 (1140)
ν_{31}	1183 (1623)	D−O−D bend	1132 (1553)	1182 (1613)	D−O−D bend + D−Cl stretch	1143 (1560)
ν_{32}	1225 (1701)	D−O−D bend	1184 (1643)	1187 (1625)	D−O−D bend + D−Cl stretch	1150 (1573)
ν_{33}	1248 (1733)	D_3O^+ bend	1204 (1672)	1201 (1650)	D−O−D bend + D−Cl stretch	1156 (1587)
ν_{34}	1626 (2190)	D_3O^+ asym O−D stretch	1671 (2250)	1218 (1679)	D−O−D bend	1170 (1612)
ν_{35}	1676 (2261)	D_3O^+ asym O−D stretch	1715 (2312)	1929 (2645)	Hb O−D stretch	2003 (2747)
ν_{36}	1846 (2582)	D_3O^+ sym O−D stretch	1916 (2679)	2099 (2883)	Hb O−D stretch	2127 (2921)
ν_{37}	2082 (2861)	Hb O−D stretch	2062 (2833)	2199 (3024)	Hb O−D stretch	2204 (3031)
ν_{38}	2100 (2886)	Hb O−D stretch	2082 (2861)	2343 (3229)	Hb O−D stretch	2311 (3185)
ν_{39}	2153 (2962)	Hb O−D stretch	2123 (2921)	2587 (3554)	free O−D stretch	2481 (3409)
ν_{40}	2595 (3566)	free O−D stretch	2475 (3400)	2604 (3578)	free O−D stretch	2485 (3414)
ν_{41}	2597 (3568)	free O−D stretch	2478 (3404)	2607 (3580)	free O−D stretch	2485 (3411)
ν_{42}	2600 (3572)	free O−D stretch	2482 (3409)	2610 (3586)	free O−D stretch	2485 (3413)

[a] See the footnote for Table 6 for additional information.

TABLE 8: Vibrational Assignment for the $n = 5$ Clusters' Spectra

	$[D(D_2O)_5]^+Cl^-$			$[DCl(D_2O)_5]$		
NM	VA	assignment	CP	VA	assignment	CP
ν_{34}	1027 (1398)	D_3O^+ bend	957 (1304)			
ν_{35}	1173 (1607)	D−O−D bend	1130 (1547)			
ν_{36}	1177 (1610)	D−O−D bend	1131 (1549)	1185 (1622)	D−O−D bend	1141 (1561)
ν_{37}	1184 (1634)	D−O−D bend	1138 (1570)	1188 (1632)	D−O−D bend	1142 (1566)
ν_{38}	1187 (1642)	D−O−D bend	1140 (1574)	1193 (1639)	D−O−D bend	1146 (1573)
ν_{39}	1205 (1673)	D−O−D bend	1153 (1600)	1204 (1654)	D−O−D bend	1138 (1562)
ν_{40}	1224 (1698)	D−O−D bend	1177 (1632)	1217 (1675)	D−O−D bend	1164 (1600)
ν_{41}	1613 (2163)	D_3O^+ asym O−D stretch	1651 (2213)	1341 (1861)	D−Cl stretch	1382 (1917)
ν_{42}	1673 (2245)	D_3O^+ asym O−D stretch	1766 (2368)	1979 (2712)	Hb O−D stretch	2028 (2780)
ν_{43}	1815 (2541)	D_3O^+ sym O−D stretch	1855 (2597)	2120 (2913)	Hb O−D stretch	2134 (2932)
ν_{44}	2056 (2823)	Hb O−D stretch	2071 (2842)	2198 (3024)	Hb O−D stretch	2186 (3006)
ν_{45}	2071 (2846)	Hb O−D stretch	2087 (2865)	2220 (3054)	Hb O−D stretch	2212 (3042)
ν_{46}	2207 (3036)	Hb O−D stretch	2185 (3006)	2418 (3346)	Hb O−D stretch	2341 (3239)
ν_{47}	2235 (3077)	Hb O−D stretch	2206 (3037)	2503 (3423)	Hb O−D stretch	2420 (3309)
ν_{48}	2598 (3568)	free O−D stretch	2481 (3409)	2597 (3568)	free O−D stretch	2484 (3412)
ν_{49}	2598 (3569)	free O−D stretch	2481 (3409)	2598 (3569)	free O−D stretch	2483 (3410)
ν_{50}	2599 (3570)	free O−D stretch	2482 (3410)	2605 (3579)	free O−D stretch	2482 (3410)
ν_{51}	2600 (3571)	free O−D stretch	2483 (3410)	2606 (3579)	free O−D stretch	2488 (3417)

TABLE 9: Vibrational Assignment for the $n = 6$ Clusters' Spectra

	$[D(D_2O)_6]^+Cl^-$			$[DCl(D_2O)_6]$		
NM	VA	assignment	CP	VA	assignment	CP
ν_{40}	1053 (1425)	D_3O^+ bend	999 (1354)			
ν_{41}	1172 (1607)	D−O−D bend	1120 (1534)			
ν_{42}	1177 (1611)	D−O−D bend	1127 (1543)	897 (1234)	D−Cl stretch	1044 (1434)
ν_{43}	1203 (1650)	D−O−D bend	1131 (1549)	1183 (1620)	D−O−D bend	1141 (1563)
ν_{44}	1211 (1661)	D−O−D bend	1145 (1571)	1193 (1636)	D−O−D bend	1147 (1573)
ν_{45}	1221 (1676)	D−O−D bend	1166 (1602)	1206 (1656)	D−O−D bend	1158 (1590)
ν_{46}	1257 (1753)	D_3O^+ bend	1227 (1710)	1209 (1659)	D−O−D bend	1164 (1599)
ν_{47}	1259 (1756)	D_3O^+ bend	1386 (1933)	1230 (1690)	D−O−D bend	1171 (1608)
ν_{48}	1549 (2074)	D_3O^+ asym O−D stretch	1534 (2055)	1232 (1692)	D−O−D bend	1182 (1624)
ν_{49}	1665 (2241)	D_3O^+ asym O−D stretch	1759 (2364)	1918 (2628)	Hb O−D stretch	1990 (2727)
ν_{50}	1818 (2540)	D_3O^+ sym O−D stretch	1950 (2725)	2155 (2960)	Hb O−D stretch	2159 (2964)
ν_{51}	2217 (3048)	Hb O−D stretch	2022 (2780)	2244 (3087)	Hb O−D stretch	2103 (2893)
ν_{52}	2234 (3073)	Hb O−D stretch	2065 (2840)	2287 (3150)	Hb O−D stretch	2254 (3104)
ν_{53}	2269 (3124)	Hb O−D stretch	2072 (2852)	2305 (3189)	Hb O−D stretch	2268 (3137)
ν_{54}	2308 (3181)	Hb O−D stretch	2120 (2922)	2358 (3222)	Hb O−D stretch	2314 (3162)
ν_{55}	2320 (3216)	Hb O−D stretch	2187 (3031)	2421 (3349)	Hb O−D stretch	2317 (3205)
ν_{56}	2370 (3233)	Hb O−D stretch	2353 (3210)	2516 (3449)	free O−D stretch	2334 (3199)
ν_{57}	2525 (3471)	free O−D stretch	2199 (3022)	2524 (3463)	free O−D stretch	2385 (3273)
ν_{58}	2536 (3486)	free O−D stretch	2479 (3407)	2601 (3573)	free O−D stretch	2486 (3416)
ν_{59}	2593 (3561)	free O−D stretch	2483 (3409)	2602 (3574)	free O−D stretch	2488 (3417)
ν_{60}	2599 (3569)	free O−D stretch	2476 (3400)	2604 (3576)	free O−D stretch	2489 (3418)

3. Clusters with n ≥ 4: Distinguishing Dissociated from Undissociated Species. As the number of water molecules in the aggregates exceeds three, the complexity of the spectra increases significantly. In Tables 7, 8, and 9, we report our assignment of the high-frequency region belonging to the dissociated and undissociated clusters for $n = 4$, 5, and 6, respectively. The most appealing feature is that dissociated clusters show the typical bands of hydronium-like stretching modes, which in all cases do not overlap with the bands of the undissociated counterparts. Likewise, the D−Cl stretching of

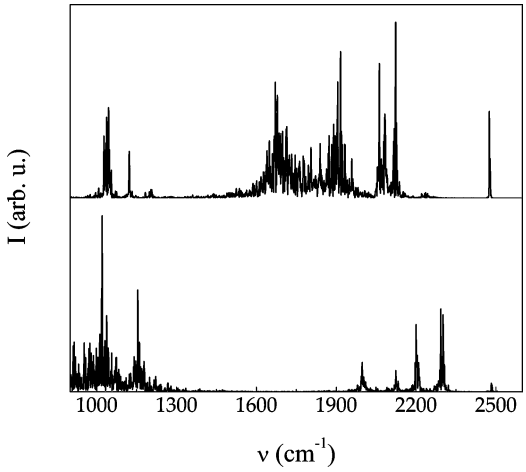

Figure 7. Vibrational spectra of the $n = 4$ dissociated (upper graph) and undissociated (lower graph) clusters (see Table 7 for the mode assignment).

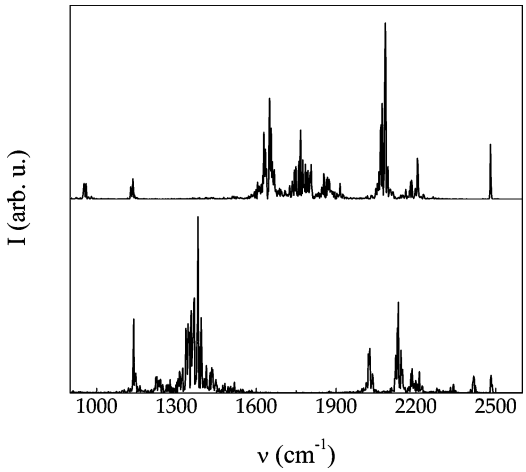

Figure 8. Vibrational spectra of the $n = 5$ dissociated (upper graph) and undissociated (lower graph) clusters (see Table 8 for the mode assignment).

the undissociated clusters is always in a region that is not congested in the corresponding dissociated cluster's spectrum. In this respect, for a given cluster size, the spectrum has a unique signature that renders it easier to distinguish between the two isomers. To appreciate this characteristic and potentially useful feature better, in Figures 7, 8, and 9, we superimpose the spectra for each isomer of a given size. It can be seen that very often D−O−D bending modes of dissociated species overlap with those of undissociated clusters. A clear trend is not found: Whereas for the $n = 4$ and 6 species the dissociated aggregates show a more pronounced red shift of some of these bands with respect to the undissociated isomers, in the case of $n = 5$ we find that the frequency range for this mode is very similar in both cases.

Another feature that can be helpful in assigning the isomer type is given by the number of hydrogen-bonded and free deuterium atoms belonging to the water molecules (see subsection IIIB). There is a net separation of at least 100 cm^{-1} between the vibrational frequencies of the O−D stretch for these two types. For $n = 4$, we can see that there are three of each kind in the dissociated cluster, while the undissociated isomer has four of each type. In the $n = 5$ cluster, we find four free deuterium atoms in the dissociated and undissociated clusters, but the former has only four hydrogen-bonded deuteriums whereas the latter has six. For $n = 6$, we find four free and six

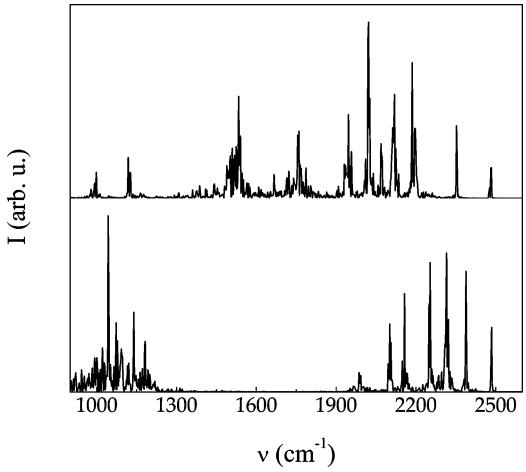

Figure 9. Vibrational spectra of the $n = 6$ dissociated (upper graph) and undissociated (lower graph) clusters (see Table 9 for the mode assignment).

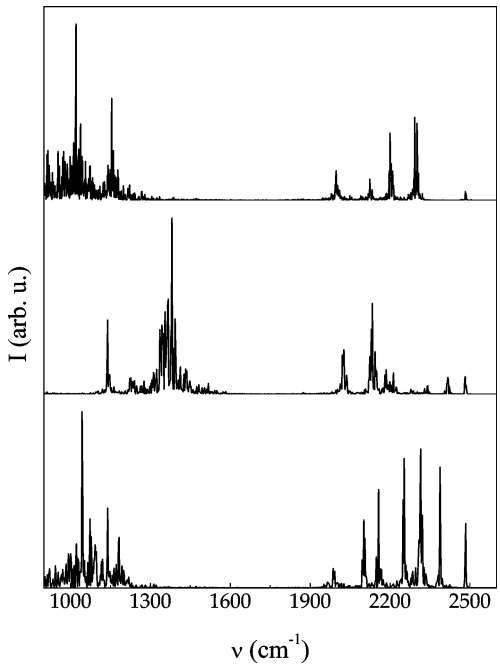

Figure 10. Vibrational spectra of the $n = 4$ (upper graph), $n = 5$ (middle graph), and $n = 6$ (lower graph) undissociated clusters.

hydrogen-bonded deuterium atoms in the dissociated cluster, while the undissociated isomer has five and seven of each type, respectively. Simulated spectra show that the vibrational frequencies of free deuterium atoms are quite similar, whereas the vibrational signatures of those deuterium atoms that are engaged in hydrogen bonds clearly differ. Thus, for well-resolved IR spectra, it might be possible to infer the number of hydrogen-bonded deuterium atoms upon comparing the qualitative features of the experimental IR spectra to those of computed ones.

In Figures 10 and 11, we compile a direct comparison of all dissociated and undissociated spectra, respectively. It can be seen that for the $n = 4$ and 6 undissociated clusters the D−Cl band is red-shifted with respect to smaller clusters, and it is also broader. While the red shift is due to a weaker interaction between chloride and deuterium, the broadening is a consequence of the deuterium fluxionality already pointed out in subsection IIIB. For $n = 5$, this normal mode is less red-shifted than that for the $n = 3$ cluster. Again this is in conjunction

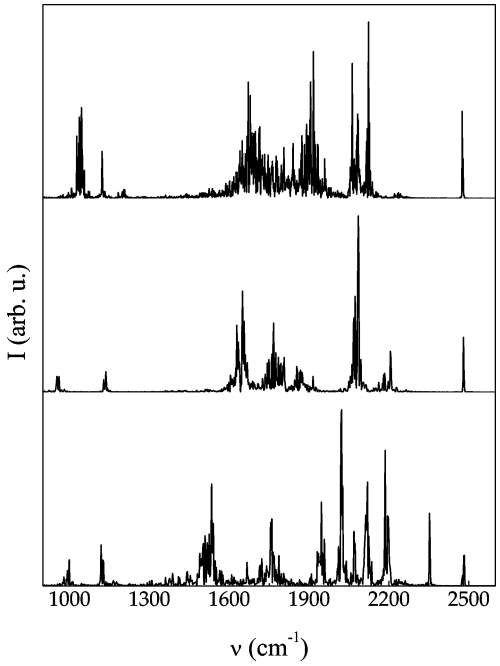

Figure 11. Vibrational spectra of the $n = 4$ (upper graph), $n = 5$ (middle graph), and $n = 6$ (lower graph) dissociated clusters.

with the trend seen for the δ probability distribution functions discussed earlier. In the case of the dissociated clusters, however, we can see that besides the differences already mentioned in the hydronium stretching region, the number of O−D vibrational bands also increases as the cluster size increases. In this case, the complexity of the interactions does not allow one to define a clear general trend in the shift experienced by these modes, and a case-by-case comparison is therefore mandatory.

Finally, we wish to mention that the present results refer to those IR spectra that are expected for the most stable isomers. There is recent evidence for a similar system that the thermodynamically stable product might not be observed at ultracold conditions.[67,68] At sufficiently low temperatures, the fragments cannot rearrange any longer to optimize the short-range chemical (e.g., hydrogen-bonding) interactions, which leads to trapping in long-range electrostatically steered arrangements.

IV. Conclusions and Outlook

It is well-appreciated that the assignment of experimental vibrational spectra of microsolvated acids, such as $DCl(D_2O)_n$ aggregates, with the aim to reveal their structure is difficult even for moderately large aggregates. However, vibrational spectroscopy is one of the primary tools that is used experimentally to elucidate the structure of such species, in particular when it comes to the question of whether the microsolvated acid is dissociated or not and precisely how the detached proton is solvated. Here, the relation between energetic, structural, and infrared spectral properties of the most stable $DCl(D_2O)_n$ neutral and zwitterionic isomers (n ranging up to six) has been studied using ab initio molecular dynamics simulations. This technique allows one to address directly structural effects caused by vibrational averaging and/or floppy motion of protons along hydrogen bonds, thus causing systematic band shifting and line shape broadening in IR spectra.

Within the investigated size range, each aggregate shows a very specific hydrogen-bond arrangement of molecules in which some interactions can uniquely characterize a given isomer. Car−Parrinello molecular dynamics simulations allowed us to investigate the dissociation of the microsolvated acid, DCl, and to relate its behavior to fluctuations in its (micro-)solvation environment. Furthermore, we found that for each hydrogen-bonding topology there is a unique signature in the IR spectra that allows us to establish a connection between structural and dynamical properties. In particular, dissociated clusters can be distinguished based on different bands present in the hydronium stretching region for a given cluster size. Undissociated clusters, however, are found to be characterized best by the behavior of the D−Cl stretching band. This is important for upcoming experimental studies because the corresponding frequencies are located in distinct spectral regions. The hydrogen-bond topology at a given cluster size and the D···O interaction weaken the D−Cl bond, causing the appearance of interesting features in the probability distribution of the proton-transfer coordinate and in the D−Cl stretching band. For small n, the consequence is just a red shift of the vibrational band, whereas for larger aggregates the proton behavior tends to become more fluxional and the red shift is accompanied by a dramatic band broadening that signals the onset of proton transfer.

An important issue arising from the study of these small aggregates concerns the comparison to experimental IR data. While this study answers questions concerning the assignment of vibrational spectra and their connection to the energetic and structural properties of the underlying hydrogen-bonded aggregates, it also poses new questions such as (i) isomerization paths, (ii) IR signatures which allow us to distinguish metastable isomers not considered here, (iii) zero-point motion effects on the fluxional behavior of the Cl−D···O hydrogen bond, and (iv) the influence of the hydrogen-bond topology on the shifts of free and hydrogen-bonded O−D stretching modes. Some of these interesting issues are currently being addressed in our laboratory.

Acknowledgment. We gratefully acknowledge a pleasant collaboration with Martina Havenith and co-workers on HCl−H_2O aggregation phenomena within the framework of the DFG Forschergruppe 681. Their experimental work on rovibrational spectroscopy of HCl, $(HCl)_2$, and HCl−H_2O is published with this article.[69] In addition, we are grateful to Professor Kwang Soo Kim for kindly having provided initial cluster structures. We also thank Sergei Ivanov, Pawel Rodziewicz, Martin Suhm for useful discussions. Partial support by DFG (FOR 618 "Molecular Aggregation'') and FCI are gratefully acknowledged as well as computer resources from Bovilab@RUB and Rechnerverbund−NRW (LiDO).

References and Notes

(1) Solomon, S.; Garcia, R. R.; Rowland, F. S.; Wuebbles, D. J. *Nature* **1986**, *321*, 755.
(2) Molina, M. J.; Tso, L. T.; Molina, L. T.; Wang, F. C. Y. *Science* **1987**, *238*, 1253.
(3) Devlin, J. P.; Uras, N.; Sadlej, J.; Buch, V. *Nature* **2002**, *417*, 269.
(4) Bianco, R.; Hynes, J. T. *Acc. Chem. Res.* **2006**, *39*, 159.
(5) Amirand, C.; Meillard, D. *J. Mol. Struct.* **1988**, *179*, 181.
(6) Weimann, M.; Fárník, M.; Suhm, M. A. *Phys. Chem. Chem. Phys.* **2002**, *4*, 3933.
(7) Huneycutt, A. J.; Stickland, R. J.; Hellberg, F.; Saykally, R. J. *J. Chem. Phys.* **2003**, *118*, 1221.
(8) Fárník, M.; Weimann, M.; Suhm, M. A. *J. Chem. Phys.* **2003**, *118*, 10120.
(9) Smith, A.; Vincent, M. A.; Hillier, I. H. *J. Phys. Chem. A* **1999**, *103*, 1132.
(10) Svanberg, M. J.; Pettersson, B. C.; Bolton, K. J. *J. Phys. Chem. A* **2000**, *104*, 5787.
(11) Chaban, G. M.; Gerber, R. B.; Janda, K. C. *J. Phys. Chem. A* **2001**, *105*, 8323.
(12) Sobolewski, A. L.; Domcke, W. *J. Phys. Chem. A* **2003**, *107*, 1557.
(13) Packer, M. J.; Clary, D. C. *J. Phys. Chem.* **1995**, *99*, 14323.

(14) Estrin, D. A.; Kohanoff, J.; Laria, D. H.; Weht, R. O. *Chem. Phys. Lett.* **1997**, *280*, 280.
(15) Buesnel, R.; Hillier, I. H.; Masters, A. J. *Chem. Phys. Lett.* **1995**, *247*, 391.
(16) Lee, C.; Sosa, C.; Planas, M.; Novoa, J. J. *J. Chem. Phys.* **1996**, *104*, 7081.
(17) Planas, M.; Lee, C.; Novoa, J. J. *J. Phys. Chem.* **1996**, *100*, 16495.
(18) Re, S.; Osamura, Y.; Suzuki, Y.; Schaefer, H. F., III. *J. Chem. Phys.* **1998**, *109*, 973.
(19) Milet, A.; Struniewicz, C.; Moszynski, R.; Wormer, P. E. S. *J. Chem. Phys.* **2001**, *115*, 349.
(20) Cabaleiro-Lago, E. M.; Hermida-Ramón, J. M.; Rodríguez-Otero, J. *J. Chem. Phys.* **2002**, *117*, 3160.
(21) Odde, S.; Mhin, B. J.; Lee, S.; Myoung, H.; Kim, K. S. *J. Chem. Phys.* **2004**, *120*, 9524.
(22) Goursot, A.; Fischer, G.; Lovallo, C. C.; Salahub, D. R. *Theor. Chem. Acc.* **2005**, *114*, 115.
(23) Odde, S.; Mhin, B. J.; Lee, K. H.; Lee, H. M.; Tarakeshwar, P.; Kim, K. S. *J. Phys. Chem. A* **2006**, *110*, 7918.
(24) (a) Goyal, S.; Schutt, D. L.; Scoles, G. *Phys. Rev. Lett.* **1992**, *69*, 933. (b) Goyal, S.; Schutt, D. L.; Scoles, G. *Phys. Rev. Lett.* **1994**, *73*, 2512.
(25) Scoles, G.; Lehmann, K. K. *Science* **2000**, *287*, 2429.
(26) Yamabe, S.; Tsuchida, N. *J. Comput. Chem.* **2003**, *24*, 939.
(27) Hermida-Ramón, J. M.; Cabaleiro-Lago, E. M.; Rodríguez-Otero, J. *Chem. Phys.* **2004**, *302*, 53.
(28) D'Auria, R.; Turco, R. P.; Houk, K. N. *J. Phys. Chem. A* **2004**, *108*, 3756.
(29) Sicilia, M. C.; Niñtildeo, A.; Muñoz-Caro, C. *J. Phys. Chem. A* **2005**, *109*, 8341.
(30) Li, S.; Weber, K. H.; Tao, F. M.; Gu, R. *Chem. Phys.* **2006**, *323*, 397.
(31) (a) Marx, D. *ChemPhysChem* **2006**, *7*, 1848. (b) Marx, D. *Chem. Phys. Chem.* **2007**, *8*, 209 (addendum).
(32) Knoll, L.; Vager, Z.; Marx, D. *Phys. Rev. A* **2003**, *67*, 022506.
(33) Car, R.; Parrinello, M. *Phys. Rev. Lett.* **1985**, *55*, 2471.
(34) Hutter, J. et al. *CPMD*, version 3.11; IBM Corp., MPI für Festköorperforschung: Stuttgart, Germany, 1990−2006, 1997−2001. http://www.cpmd.org.
(35) Marx, D.; Hutter, J. In *Modern Methods and Algorithms of Quantum Chemistry Proceedings*, 2nd ed.; Grotendorst, J., Ed.; John von Neumann Institut für Computing 3; Forschungszentrum Jülich: Jülich, Germany, 2000.
(36) Becke, A. D. *Phys. Rev. A* **1988**, *38*, 3098.
(37) Lee, C.; Yang, W.; Parr, R. G. *Phys. Rev. B* **1988**, *37*, 785.
(38) Troullier, N.; Martins, J. L. *Phys. Rev. B* **1991**, *43*, 1993.
(39) Hockney, R. W. *Methods Comput. Phys.* **1970**, *9*, 136.
(40) Martyna, G. J.; Klein, M. L.; Tuckerman, M. E. *J. Chem. Phys.* **1992**, *97*, 2635.
(41) Martyna, G. J.; Hughes, A.; Tuckerman, M. E. *J. Chem. Phys.* **1999**, *110*, 3275.
(42) Blöchl, P. E. *Phys. Rev. B* **1994**, *50*, 17953 (see in particular subsection V.C.2 therein).
(43) Marx, D.; Hutter, J.; Parrinello, M. *Chem. Phys. Lett.* **1995**, *241*, 457.
(44) Marx, D.; Fois, E.; Parrinello, M. *Int. J. Quantum. Chem.* **1996**, *57*, 655.
(45) Fukui, K.; Cline, J. I.; Frederick, J. H. *J. Chem. Phys.* **1997**, *107*, 4551.
(46) Kumar, P. P.; Marx, D. *Phys. Chem. Chem. Phys.* **2006**, *8*, 573.
(47) Marzari, N.; Vanderbilt, D. *Phys. Rev. B* **1997**, *56*, 12847.
(48) Silvestrelli, P. L. *Phys. Rev. B* **1999**, *59*, 9703.
(49) Berghold, G.; Mundy, C. J.; Romero, A. H.; Hutter, J.; Parrinello, M. *Phys. Rev. B* **2000**, *61*, 10040.
(50) Berens, P. H.; Wilson, K. R. *J. Chem. Phys.* **1981**, *74*, 4872.
(51) Berens, P. H.; White, S. R.; Wilson, K. R. *J. Chem. Phys.* **1981**, *75*, 515.
(52) Berens, P. H.; Mackay, D. H. J.; White, G. M.; Wilson, K. R. *J. Chem. Phys.* **1983**, *79*, 2375.
(53) Ramírez, R. P.; López-Ciudad, T.; Kumar, P.; Marx, D. *J. Chem. Phys.* **2004**, *121*, 3973.
(54) Rousseau, R.; Kleinschmidt, V.; Schmitt, U. W.; Marx, D. *Angew. Chem., Int. Ed.* **2004**, *43*, 4804.
(55) Asvany, O.; Kumar, P.; Redlich, P, B.; Hegemann, I.; Schlemmer, S.; Marx, D. *Science* **2005**, *309*, 1219.
(56) Mathias, G.; Marx, D. *Proc. Natl. Acad. Sci. U.S.A.* **2007**, *104*, 6980.
(57) Wilson, E. B., Jr.; Decius, J. C.; Cross, P. C. In *Molecular Vibrations: The Theory of Infrared and Raman Vibrational Spectra*; McGraw-Hill: New York, 1955.
(58) Martinez, M.; Gaigeot, P. M.; Borgis, D.; Vuilleumier, R. *J. Chem. Phys.* **2006**, *125*, 144106.
(59) Van Duijneveldt, F. B. In *Molecular Interactions: From van der Waals to Strongly Bound Complexes*; Scheiner, S., Ed.; Wiley: New York, 1997; pp 81−104.
(60) Frisch, M. J.; Trucks, G. W.; Schlegel, H. B.; Scuseria, G. E.; Robb, M. A.; Cheeseman, J. R.; Montgomery, J. A., Jr.; Vreven, T.; Kudin, K. N.; Burant, J. C.; Millam, J. M.; Iyengar, S. S.; Tomasi, J.; Barone, V.; Mennucci, B.; Cossi, M.; Scalmani, G.; Rega, N.; Petersson, G. A.; Nakatsuji, H.; Hada, M.; Ehara, M.; Toyota, K.; Fukuda, R.; Hasegawa, J.; Ishida, M.; Nakajima, T.; Honda, Y.; Kitao, O.; Nakai, H.; Klene, M.; Li, X.; Knox, J. E.; Hratchian, H. P.; Cross, J. B.; Bakken, V.; Adamo, C.; Jaramillo, J.; Gomperts, R.; Stratmann, R. E.; Yazyev, O.; Austin, A. J.; Cammi, R.; Pomelli, C.; Ochterski, J. W.; Ayala, P. Y.; Morokuma, K.; Voth, G. A.; Salvador, P.; Dannenberg, J. J.; Zakrzewski, V. G.; Dapprich, S.; Daniels, A. D.; Strain, M. C.; Farkas, O.; Malick, D. K.; Rabuck, A. D.; Raghavachari, K.; Foresman, J. B.; Ortiz, J. V.; Cui, Q.; Baboul, A. G.; Clifford, S.; Cioslowski, J.; Stefanov, B. B.; Liu, G.; Liashenko, A.; Piskorz, P.; Komaromi, I.; Martin, R. L.; Fox, D. J.; Keith, T.; Al-Laham, M. A.; Peng, C. Y.; Nanayakkara, A.; Challacombe, M.; Gill, P. M. W.; Johnson, B.; Chen, W.; Wong, M. W.; Gonzalez, C.; Pople, J. A. *Gaussian 03*, revision C.02; Gaussian, Inc.: Wallingford, CT, 2004.
(61) Ferrario, M.; Haughney, M.; McDonald, I. R.; Klein, M. L. *J. Chem. Phys.* **1990**, *93*, 5156.
(62) Rey, R.; Møller, K. B.; Hynes, J. T. *J. Phys. Chem. A* **2002**, *106*, 11993.
(63) Scheiner, S. *Hydrogen Bonding: A Theoretical Perspective*; Oxford University Press: New York, 1997.
(64) Desiraju, G. R.; Steiner, T. *The Weak Hydrogen Bond in Structural Chemistry and Biology*; International Uniion of Crystallography Monographs on Crystallography 9; Oxford University Press: New York, 1999.
(65) Bondi, A. *J. Phys. Chem.* **1964**, *68*, 441.
(66) Lindsay, C. M.; Douberly, G. E.; Miller, R. E. *J. Mol. Struct.* **2006**, *786*, 96.
(67) Madeja, F.; Havenith, M.; Nauta, K.; Miller, R. E.; Chocholoušovà, J.; Hobza, P. *J. Chem. Phys.* **2004**, *120*, 10554.
(68) Gantenberg, M.; Halupka, M.; Sander, W. *Chem.—Eur. J.* **2000**, *6*, 1865.
(69) Ortlieb, M.; Birer, Ö.; Letzner, M.; Schwaab, G. W.; Havenith, M. *J. Phys. Chem. A* **2007**, *111*, 12192.